Comprehensive methodology for tracking burning firebrands in a vertical wind tunnel using multi-view video analysis

Misarah Abdelaziz^{A,*} and Andrew, L. Sullivan^A

For full list of author affiliations and declarations see end of paper

*Correspondence to:

Misarah Abdelaziz CSIRO, GPO Box 1700, Acton, Canberra, ACT 2601, Australia

Email: E misarah.abdelaziz@csiro.au

Received: 17 June 2025 Accepted: 22 September 2025 Published: 17 October 2025

Cite this: Abdelaziz M and Sullivan AL (2025) Comprehensive methodology for tracking burning firebrands in a vertical wind tunnel using multi-view video analysis. International Journal of Wildland Fire 34, WF25153. doi:10.1071/WF25153

© 2025 The Author(s) (or their employer(s)). Published by CSIRO Publishing on behalf of

This is an open access article distributed under the Creative Commons Attribution 4.0 International License (CC BY).

OPEN ACCESS

ABSTRACT

Background. Burning debris (firebrands) can potentially travel significant distances to ignite spot fires many kilometres downwind of a wildfire, posing substantial challenges for fire spread prediction and management. Aim. To improve our understanding of the combustion and flight behaviours of common bark firebrands through better quantification and detailed analysis of their motion, combustion and aerodynamic behaviour. Methods. A custom firebrand tracking system consisting of three synchronised video cameras positioned orthogonally around the working section of a vertical wind tunnel was built and bespoke image processing algorithms developed to automatically reconstruct the 3D trajectory and combustion behaviour of a bark sample. Key results. The system was found to accurately estimate bark sample position as well as spatial velocity, orientation changes and burnout profile. Conclusions. A robust and accurate methodology to track the dynamic trajectory and behaviour of untethered burning bark falling at its terminal velocity was developed that overcomes many of the limitations of previous tracking approaches. Implications. This study, applicable to a broad range of bark species as well as other firebrand materials under varying conditions, enables the development of more accurate predictive models of firebrand transport that will help improve the simulation and prediction of spotting in wildfires.

Keywords: 3D trajectory, bushfire behaviour, combustion dynamics, computer vision, fluid mechanics experiment, image processing algorithm, inconsistent particle tracking, spotfire, spotting.

Introduction

Spot fires initiated by firebrands or embers - flaming, glowing or smouldering fragments of vegetative debris ignited in a firefront - pose a significant challenge to wildfire management and suppression. Spot fires can occur well ahead of the main firefront, greatly enhancing the rate of wildfire spread, increasing fireline intensity and breaching suppression efforts (Sullivan 2017). Spotting is recognised as a major mechanism driving wildfire propagation in many vegetation types, and has been directly linked to the destruction of homes and other property during wildfires (McArthur 1969; Filkov et al. 2023).

Firebrand transport can occur over a range of distances, depending on the mechanisms involved (Sullivan et al. 2012). Firebrands blown directly out of the flame zone by the wind cause short-distance spotting, distances typically tens to hundreds of metres from the originating fire. These exacerbate fire spread locally, greatly increase suppression difficulty and firefighter safety concerns, and are often described as 'ember storms' when they occur in very large numbers. Conversely, firebrands that become entrained in a fire's convection column can be lofted to significant heights before they fall out and are transported by the prevailing wind to start spot fires downwind when they land alight. Spot fires ignited by such lofted firebrands up to 5 km from the originating fire are considered medium distance, whereas those that start in excess of 5 km are long distance. Medium and long distance spotting significantly complicate suppression efforts, allowing a fire to cross substantial breaks in fuel and topography (McArthur 1967; Cruz et al. 2015).

In this paper, we use the term firebrand to refer to the large burning bark particles under study. Smaller burning fragments are referred to as embers.

The aerodynamic properties and burnout times of firebrands - key factors influencing spotting potential - are affected by their size, shape and composition (Ellis 2000). Australian eucalypt forests are especially notorious for their intense spotting behaviour (Ellis 2011). Eucalyptus bark, particularly stringybark and ribbon bark, is known for its propensity to generate effective firebrands owing to its morphology and combustion characteristics (McArthur 1967; Tolhurst and Cheney 1999; Hines et al. 2010). Smooth gum bark species such as ribbon bark are typically associated with reports of spotting distances exceeding 30 km under extreme wildfire conditions (Cruz et al. 2012; Hall et al. 2015). Analysis of the 1962 Daylesford fire in stringybark forest revealed that short-range spotting increased fire spread rates by a factor of three (McArthur 1967; Wadhwani et al. 2022).

Although the state of the fuel bed in which a firebrand lands and the micrometeorology at the landing site, as well as the dominant mode of combustion of the firebrand when it lands all play significant roles in determining spotting potential (Ellis 2011, 2015), understanding the factors that govern firebrand transport and viability, including aerodynamic properties and burnout times, is essential for accurately predicting how far a firebrand might travel and be viable (Ellis 2000; Koo et al. 2010). Aerodynamic properties determine the firebrand's coefficient of drag and its terminal velocity (the vertical velocity at which the drag force balances the effective weight of the firebrand, corresponding in the wind tunnel to the speed at which the firebrand remains at a constant height), whereas burnout time determines how far a firebrand can travel while retaining the ability to ignite a fuel bed under conducive conditions (i.e. viability).

Previous studies have explored some of these aspects using small untethered firebrands in wind tunnel experiments. For example, Ellis (2013) demonstrated that most messmate firebrands burn out within 180 s of full flaming ignition, corresponding to transport distances of several kilometres under modelled conditions. Hall *et al.* (2015) studied the combustion times and terminal velocities of three bark morphologies of *Eucalyptus viminalis*: flat plates, simple cylinders and internally convoluted cylinders. They found internally convoluted cylinders had the longest burnout times, often in excess of 20 min, which, along with their low terminal velocity, could enable spotting distances of over 20 km. This study provided the first empirical evidence supporting the long-distance spotting potential of this bark type.

Tohidi and Kaye (2017) investigated the free-fall aerodynamic behaviour of non-combusting rod-like firebrands and validated a three-dimensional (3D) deterministic six-degrees-of-freedom (6-DOF) transport model. Their findings high-lighted the necessity of including complete 6-DOF aerodynamics to accurately predict firebrand flight characteristics.

Accurately characterising firebrand aerodynamic and combustion behaviour is essential for improving fire spread models, mitigating the impacts of wildfires and safely conducting prescribed burning. However, firebrands are influenced by turbulent atmospheric conditions, spatially and temporally varying wind fields, and interactions with convective fire plumes, making their transport dynamics highly complex. Although experimental and computational studies have attempted to address many of these challenges, gaps remain. Laboratory-scale experiments, using vertical wind tunnels, provide valuable insights but are often limited to small firebrands or firebrands that are tethered, leaving questions unanswered regarding the transport dynamics and burnout behaviour of larger firebrands (Petersen and Banerjee 2024). Furthermore, many such empirical studies were often limited in their ability to accurately measure critical attributes and variables, particularly of firebrands exhibiting highly dynamic, chaotic aerodynamic and combustion behaviours. Typically, such studies resorted to reporting average values for flight and combustion times (e.g. Ellis 2000) with a corresponding reduction in resulting model fidelity.

Computerised video-based analysis methods have emerged as powerful tools for studying the highly dynamic aerodynamic and combustion behaviour of free-falling untethered firebrands experimentally, most often in a wind tunnel. Video-based particle tracking allows detailed analysis of a firebrand's trajectory, orientation and combustion mode. However, the unique challenges associated with firebrand tracking include variations in colour, size, shape, direction and velocity, as well as the limitations of existing object-tracking algorithms designed for applications like traffic management or facial recognition. Addressing these challenges requires customised detection and tracking methodologies capable of capturing the complex dynamics of firebrand transport in thermal and visual video recordings (e.g. NIST work) (Carranza and Zhang 2017).

Filkov and Prohanov (2019) developed custom software to detect, track and analyse the behaviour of small freemoving firebrands (embers) in the field within a volume 1.5 m wide \times 1.5 m high \times 1.0 m deep using thermal imaging techniques. The software utilised bespoke filters to identify the location of embers within each frame of a thermal video and compared embers across frames based on similarity of shape and trajectory to provide unique identifiers for ember tracking. The software was found to consistently under-represent the firebrand number compared with expert observations of the same video, but the error was less than 12%, suggesting the method was promising. Almeida et al. (2021) used Particle Image Velocimetry (PIV) to investigate firebrands lofted from small burning trees, quantifying their number, sizes and velocities while also linking firebrand production to tree mass loss and defining a reaction time between peak flame height and firebrand release.

Bouvet *et al.* 2021 introduced the 'emberometer', a portable 3D diagnostic tool for characterising airborne firebrands in wildland–urban interface fires. This system combines 3D particle tracking velocimetry with 3D particle shape reconstruction to resolve firebrand trajectories and geometries, and was demonstrated in controlled firebrand showers with hundreds of

particles tracked over seconds. Field experiments reported by Petersen and Banerjee (2024) provided the first *in situ* characterisation of firebrands from real fuels, where both kinematics during lofting and post-landing physical properties were examined. Over 86,000 embers were imaged systematically, yielding particle size, aspect ratio and shape complexity statistics, with results showing mostly mildly elongated geometries and highlighting the need for further 3D shape analysis. Although many of these methods are powerful for bulk statistical characterisation of showers of firebrands, they do not resolve the detailed trajectory and burning behaviour of a single firebrand falling at its terminal velocity necessary for determining the maximum distance a viable firebrand may travel.

Although optical tracking and imaging provide some improved capabilities, issues such as firebrand deformation, occlusion, flame interference and fragmentation during flight complicate particle recognition. Furthermore, single-camera systems fail to capture full 3D trajectories and changes in orientation.

The current study aims to tackle these limitations by developing a robust, multi-view method for tracking burning untethered, free-falling bark segments in a vertical wind tunnel. The system integrates synchronised imaging from three orthogonal high-resolution cameras using custom algorithms for particle position processing and trajectory reconstruction. The goal is to enable precise automated measurement of a bark sample's position, trajectory, velocity, flaming duration and burnout time – critical inputs for modelling the transport behaviour and ignition potential of firebrands and thus spotting in wildfires.

Experimental methodology

Vertical wind tunnel setup

The CSIRO Vertical Wind Tunnel, located in the CSIRO National Bushfire Behaviour Research Laboratory in Canberra, ACT, is 11 m tall with a 4 m tapered working section (Fig. 1). It was used to study the combustion and aerodynamic behaviour of the bark samples. This facility has been used extensively in previous research on firebrand dynamics (e.g. Ellis 2000, 2010, 2013; Hall et al. 2015) and is described in detail in Knight (2001) and Knight et al. (2001). A variable speed backward-inclined centrifugal blower delivers a maximum flow rate of 11 m³ s⁻¹ at a pressure of 650 Pa, generating a maximum air velocity of 20 m s⁻¹ in the tapered working section. The working section consists of two modules, each 2125 mm long, giving a total length of 4250 mm, with a divergence to stabilise burning firebrands when at terminal velocity. Two acrylic windows, measuring 525 mm in width and 1980 mm in length, in each working section module allow direct observation and video recording of firebrand samples in flight. Instrument slots in one window facilitate sensor insertion

into the working section. A perforated aluminium screen at the base of the working section modifies the flow structure within this section, further mitigating sample-to-wall collisions and trapping of samples within the wall boundary layer, aiding accurate velocity mapping. Bark samples are introduced into the working section through a small access hatch, which is closed as soon as the sample is released into the air flow. Additional details regarding the wind tunnel and the experimental setup are available in Abdelaziz and Sullivan (2024).

Characterisation of the airflow within the test section of the CSIRO Vertical Wind Tunnel was given in detail in Abdelaziz and Sullivan (2024). In brief, the central region of the test section (extending approximately 300 mm from each wall) exhibits uniform flow, with mean air speeds adjustable between 0 and 20 m s $^{-1}$ and turbulence intensities below 0.4% under the operating conditions of the present study. These conditions provide stable and repeatable aerodynamics for firebrand tracking. Furthermore, a mapping function derived from the continuity equation enables calculation of the air velocity at any location in the working section based on the set fan speed, allowing estimation of a firebrand's terminal velocity from its vertical position at any time.

Environmental parameters, including air temperature, relative humidity and atmospheric pressure, are recorded using a CR1000 data logger (Campbell Scientific) at a sampling frequency of 5 Hz. Temperature and humidity are measured via two Vaisala HMP110 sensors positioned in the observation room and at the tunnel exit. Atmospheric pressure is monitored using a Vaisala PTB110 barometer.

Two 12-W 6000-K dimmable LED light strips were fitted into the corners of the working section to ensure optimal illumination for video recording. An orthogonal multi-camera system consisting of three 4 MP LightHunter Intelligent Bullet Network cameras (IPC264SA-DZK) was used to capture the motion of untethered, free-falling firebrands from side, front and overhead perspectives. The front-view camera provides x and z coordinates of the sample, the left-view camera provides y and z coordinates, while the top-view camera provides x and y coordinates. These low-light-capable cameras capture video at 2688 \times 1520 resolution at 30 fps.

Bark sample selection, preparation and characteristics

Large slabs of bark were manually harvested from a messmate stringybark (*Eucalyptus regnans*) in central Victoria, Australia, to develop and evaluate the performance of a bespoke tracking algorithm specifically for the CSIRO Vertical Wind Tunnel. Samples were collected from heights ranging between 0.5 and 1.5 m on unburnt trees with intact, uncharred bark. Only the outermost decorticating and loose layers were taken, leaving the cambium layer undisturbed. The harvested bark slabs were cut into a number of uniform smaller segments of 10, 15 and 20 cm lengths using a ruler

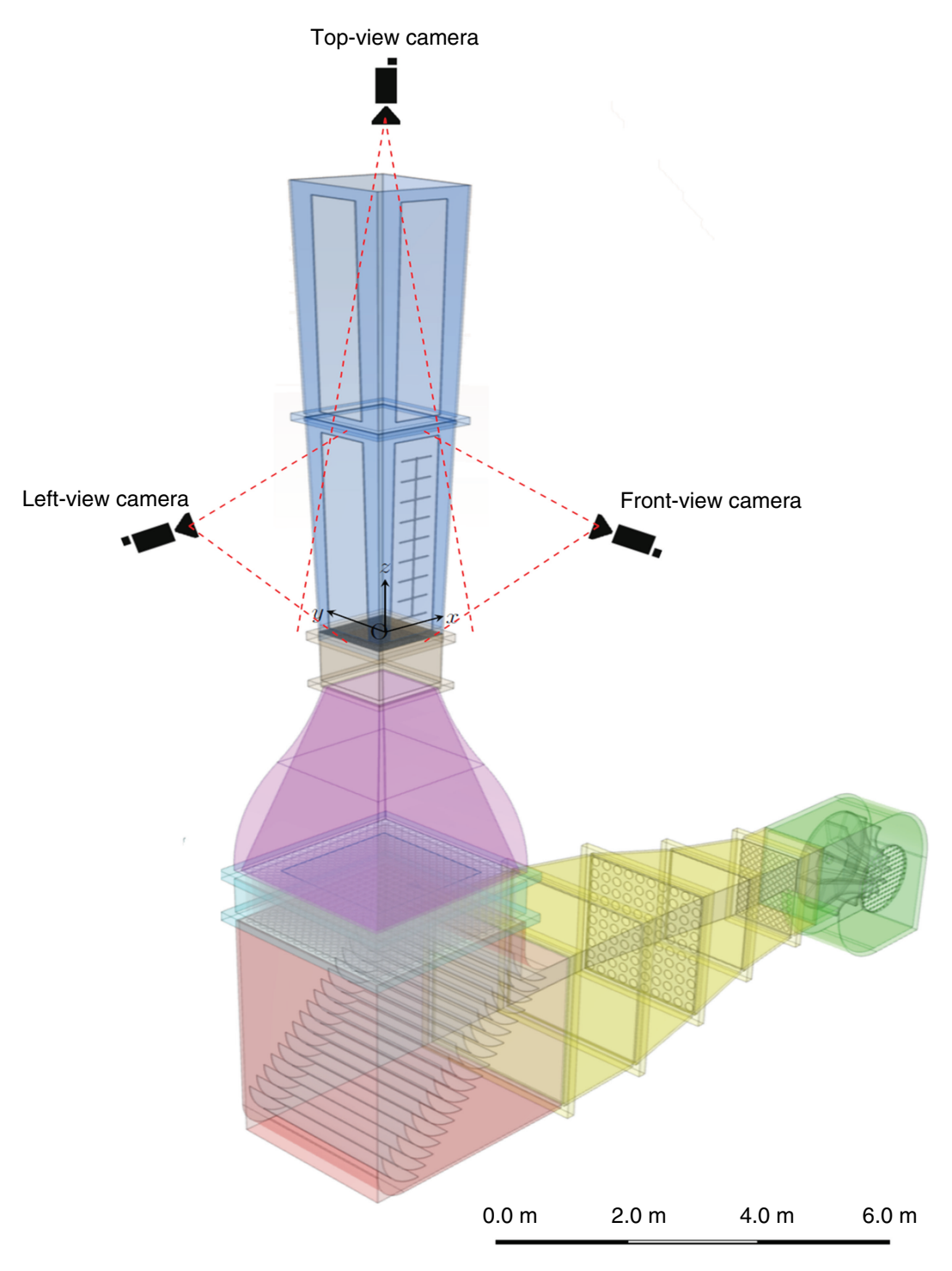


Fig. 1. A schematic of the CSIRO vertical wind tunnel adapted from Abdelaziz and Sullivan (2024). Major components are centrifugal blower (green), diffuser (yellow), turning section (red), straightening section (cyan), contrator (purple), adaptor (brown) and working section (blue).

and a handsaw or compound slide saw. Although test samples of 10, 15 and 20 cm length were prepared, only the 10 cm samples are reported in this study, as the focus here is on developing and validating the tracking algorithm. The natural width of each piece was preserved to maintain the

sample's original structure and integrity. The dimensions (length, width, depth) of each bark sample were measured using callipers and verified using a custom MATLAB algorithm for high-accuracy estimation of surface area and volume based on image analysis (see Fig. 2). Samples were

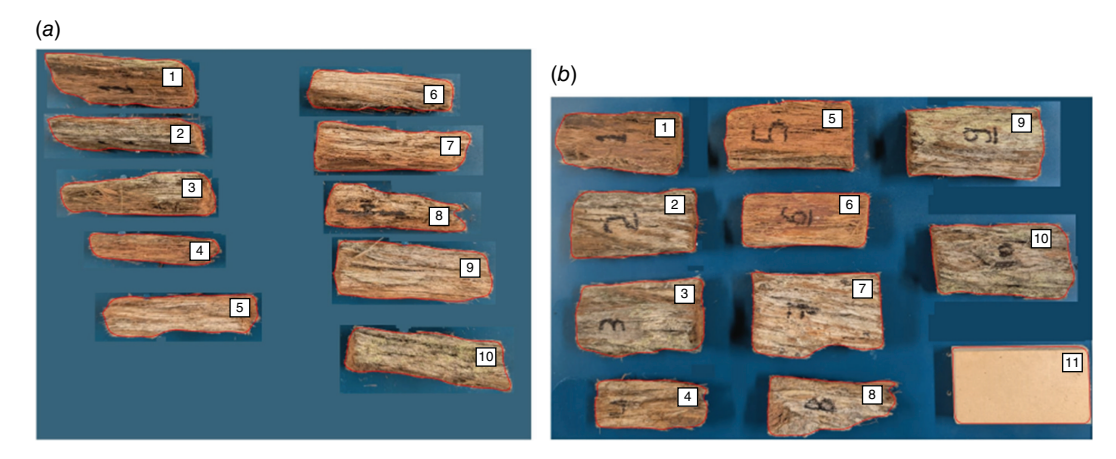


Fig. 2. Photograph of 10 selected bark samples for tracking algorithm development and evaluation. (a) Side view of samples used to obtain depth and length. (b) Top view showing the width and area of the largest face surface. The rectangular wooden piece labelled '11' in (b) serves as a reference object with known dimensions.

oven-dried at 40°C for a minimum of 24 h to simulate a bark condition typical of hot summer weather. All samples were kept in the oven until just before ignition and then weighed using a precision balance (A&D FX-3000 WP) to provide wet mass. Random samples from each length class were oven dried at 105°C for 24 h to determine the average moisture content, which was found to be 4.6% in this study. Dry mass for the remainder of the length class was then estimated using this moisture content. Table 1 summarises the characteristics of the 10 messmate stringybark samples used in the experiments.

Samples were ignited using a propane camping burner. Each sample was supported on wire arms and ignited for a consistent ignition duration to ensure full-flame immersion and consistent flaming behaviour. Once fully involved in flame, the sample was inserted into the working section through the access hatch using forceps. The fan speed was initially set approximately to each sample's terminal velocity, based on prior experiments. Minimal adjustments were made during sample insertion to keep the burning bark within the lower 2 m of the working section, where the front and left-view cameras captured its motion. Each video segment was trimmed to start immediately after insertion and access hatch closure, ensuring synchronised frames across all camera views. Any subsequent adjustments of the fan speed during the experiment were recorded, providing the actual airspeed values throughout the run.

Tracking algorithm development and validation

A custom MATLAB (2023) program was developed to analyse the video data and track the motion of a firebrand free-falling at its terminal velocity in three dimensions from which flight characteristics, such as firebrand velocity and trajectory, could be extracted and analysed.

Camera configuration and synchronisation

Each camera was individually calibrated using a laminated A4-size chequerboard pattern (10×7 grid, 25 mm square size). The board was placed at various positions and orientations within each camera's field of view, and approximately 15 images per camera were captured. MATLAB's Camera Calibration app was then used to detect corners and compute intrinsic (e.g. focal length, principal point, distortion coefficients) and extrinsic (rotation, translation) parameters.

After aligning their system times, all three cameras were started simultaneously using the EZStation software (Zhejiang Uniview Technologies Co., Ltd. 2021). Despite efforts to ensure absolute synchronisation in this manner, a one-to-two-frame lag still occurred owing to onboard processing delays. To address this, the working section lighting was briefly turned off to create a dark frame for camera synchronisation. Synchronisation was confirmed by checking the frame alignment when the lights were turned back on.

The length of each video segment was trimmed to begin immediately after bark insertion and access hatch closure, ensuring the bark appeared on the same time-synchronised frame across all camera views. Further details and figures are given in the Appendix 1.

Bark tracking procedure

Each video frame was processed sequentially. Lens distortion was corrected using the MATLAB undistortImage function (MATLAB 2023) and the set of intrinsic parameters previously obtained. Frames were cropped to focus on particular regions of interest (ROI) around the sample. In the first frame, the bark's initial position was manually marked to avoid confusion caused by internal reflections on the observation windows, particularly in the top camera view. The boundary was then defined, and the centroid of the bark's position calculated.

From the second frame onward, the algorithm calculated the absolute colour difference between consecutive frames.

Table 1. Major characteristics of bark samples used in this study. $^{ extsf{A}}$

ID	(cm)	W (cm)	D (cm)	AR, (L/W)	AR ₂ (L/D)	AR ₃ (W/D)	A ₁ (cm ²)	$A_2 (cm^2)$	A ₃ (cm ²)	V (cm³)	SA/V (cm ⁻¹)	M _w (g)	M _d (g)	ρ (kg m ⁻³)
10	10	5.3	3.7	1.9	2.7	1.4	38	31	14	961	8.0	13.2	12.6	064
02	01	6.0	2.5	1.7	4.0	2.4	43	23	=	152	1.0	15.6	14.9	860
03	01	6.3	2.8	1.6	3.6	2.3	48	76	13	180	1.0	7.7.2	26.5	147
94	60	4.2	2.3	2.0	3.7	1.8	28	15	80	083	1.2	0.60	9.80	103
90	01	0.9	4.0	1.7	2.6	1.5	45	76	23	245	8:0	16.8	16.0	990
90	01	4.6	3.3	2.1	3.0	1.4	36	24	Ε	149	1.0	12.8	12.3	082
07	01	9.9	3.3	1.6	3.1	2.0	22	30	16	224	6:0	20.4	19.5	087
80	01	4.6	2.8	2.1	3.4	1.6	32	23	80	124	1.0	15.5	14.8	120
60	=	0.9	4.0	1.8	2.7	1.5	20	39	71	254	8.0	26.4	25.2	660
01	Ε	5.8	4.6	1.9	2.4	1.3	52	34	20	296	0.7	27.1	25.9	087
AL is th	ne length, M	/ is the widt	h, D is the d	epth, AR is the	aspect ratio, A is	s the area, V is tl	ne volume, SA	A is the surface	e area, M _w is t	the wet mass	^{A}L is the length, W is the width, D is the depth, AR is the aspect ratio, A is the area, V is the volume, SA is the surface area, M_{w} is the wet mass, M_{d} is the dry mass and ρ is the density	ass and $ ho$ is	the density.	

This technique calculates the pixel-wise difference between consecutive video frames, enabling the detection of regions where movement has occurred. Thresholding this difference generated binary masks (background and pixels of interest), highlighting regions of change and thus motion. Candidate sample locations (pixels of interest) were filtered based on proximity to the previous centroid; if no nearby points were found, all candidates were retained.

The algorithm further refined centroid estimation by iteratively removing distant points and recalculating the current centroid. Additional filtering in the top view removed extraneous points caused by glass reflections. Cleaned centroids and bounding boxes were stored across frames.

For enhanced analysis, the ROI was updated dynamically. Frames were converted to hue/saturation/value (HSV) colour space, and a classification function was applied to identify the bark's burning phase (i.e. flaming, glowing, or smouldering), which was recorded for each frame.

Validation

To validate the performance of the MATLAB-based tracking algorithm, an evaluation dataset was created by manually annotating a subset of images using the Computer Vision Annotation Tool (CVAT) within MATLAB (2023). In this process, the precise position of the primary bark sample in each video frame was manually identified and annotated using rectangular bounding boxes defined by two diagonally opposing corners. To ensure annotation consistency and mitigate the effects of perspective variation, separate annotation tasks were created for each of the three camera views. The resulting annotated datasets, containing precise bounding box coordinates for the bark sample across multiple frames, were exported in CSV format and compared with the 3D point cloud generated by the firebrand tracking algorithm. The quantitative results of this comparison, including positional and trajectory errors, are presented in the Results and discussion section.

Challenges in tracking the flight of burning bark

Tracking burning bark in a vertical wind tunnel presents several unique challenges for automated vision analysis, primarily due to the experimental setup and environmental factors that affect the visibility and motion of the bark. These challenges must be addressed to ensure accurate and reliable trajectory data. The following section highlights key difficulties encountered during the tracking process and the methods employed to overcome them.

Firebrand sample occlusion

One of the primary challenges faced during this study was the partial occlusion of the burning bark by the wind tunnel structure and the surrounding laboratory. The front and leftview cameras, installed external to the tunnel with a view through each of the 1940×500 mm acrylic observation

windows, often experienced difficulty in tracking the bark when it moved into the corners of the working section. Specifically, the window mount could obscure the bark sample in the image frame, resulting in periods of missing data. Additionally, the wind tunnel laboratory's construction itself introduced an additional tracking challenges. A steel support beam for the floor above obstructed a small part of the camera's field of view (approximately 100 mm of the top of the view), limiting the ability to capture the bark's motion at higher positions in the wind tunnel. This obstruction was particularly problematic when tracking the early stages of the bark's ascent or descent.

To mitigate this issue, the calculated trajectory of the burning bark was divided into distinct continuous segments. Each segment was defined by the first and last frame in which the bark was visible in both horizontal camera views (i.e. the front and side cameras were used for 3D trajectory reconstruction; the top view camera was used only for reference and combustion phase classification). For frames where the bark was visible in both cameras, the trajectory was plotted as a dashed coloured line, the colour being related to time since commencement of the experiment. Where the bark was visible in only one camera view, the trajectory was plotted as a solid black line, representing the data that was incomplete owing to occlusion. This approach allowed continuous tracking of the sample even when partially occluded, while ensuring that the analysis was based only on the most complete data available. If the sample was occluded in both camera views, no data were collected.

Camera alignment and pixel scaling differences

Another challenge arose from the slight differences in the relative positioning of the two side-facing cameras mounted on the internal walls of the laboratory, due to the noncentred position of the tunnel within the lab. The left-side camera is positioned slightly farther from the wind tunnel's working section than the front-side camera. This positioning asymmetry introduced a minor difference in pixel scaling between the two views. This difference made it difficult to align the two camera images perfectly when placed side by side for comparison.

Although this camera asymmetry affected the visual appearance of the trajectory, it did not significantly impact the accuracy of the trajectory measurements or the movement dynamics of the burning bark. To address this issue, the data were carefully processed and re-aligned using the camera calibration parameters. Although visual inconsistencies remained, the overall trajectory analysis remained robust with minimal impact on the final results.

Sample morphological and appearance changes during combustion

Particle tracking algorithms are generally designed to monitor the position and movement of objects over a sequence of

video frames. These algorithms typically rely on identifying unique features of the object being tracked, such as colour, shape, texture, or motion patterns, and use these features to detect, predict and update the object's location as it moves in subsequent frames. For instance, tracking a red ball moving against a contrasting background involves detecting the ball's location based on its distinctive red colour and round shape. Algorithms such as template matching or colour-based tracking (e.g. using HSV colour space) then identify the ball's position in each frame. Once detected, techniques like Kalman filters or particle filters are often applied to predict its future position, account for noise and ensure smooth tracking even when the ball briefly disappears or overlaps with other objects (Prevost *et al.* 2007).

For a white car crossing a scene, the algorithm might use edge detection or feature point matching, combined with motion estimation, to follow the movement of the car. Optical flow methods can estimate the motion of the car by analysing changes in pixel intensity across frames, while more advanced techniques, such as deep learning-based object trackers (e.g. YOLO or SORT), can detect and track the car by leveraging pre-trained models that recognise vehicles (Bathija and Sharma 2019; Diwan et al. 2023). These advanced trackers not only identify the car but can also assign a unique ID to maintain its trajectory across complex scenes, even in the presence of occlusions or other vehicles. The success of the tracking process depends on factors such as the object's distinctiveness, background complexity and the robustness of the algorithm in handling challenges like lighting changes or partial obstructions.

Tracking burning bark presents unique challenges that make traditional tracking techniques unsuitable. Unlike objects such as a red ball or a white car, burning bark exhibits chaotic motion, irregular and inconsistent initial shapes, and dynamic changes in appearance due to combustion and the consumption of mass (Fig. 3). Its erratic movement in turbulent airflow makes predicting its trajectory difficult, while the lack of a consistent shape or colour complicates the use of standard labelling methods like colour segmentation or edge detection. To address these limitations, the frame-difference approach is used as a step to highlight ROI, which are then further analysed using advanced filtering and processing techniques. This integration ensures a more robust tracking system capable of handling the complexities associated with tracking burning bark in such a challenging environment.

Noise reduction and signal filtering

Noise filtering is one of the critical challenges in tracking burning bark owing to the dynamic and visually noisy environment in which it moves. The turbulent airflow combined with dynamic visual interference from flames, smoke and ash introduce significant noise into the tracking process. Small embers or bark fragments that break off from the main



Fig. 3. A video frame from the top-view camera showing a burning bark sample illustrates the challenges posed by changes in bark shape and colour, small fragments broken off from the main bark and reflection from the side window during combustion.

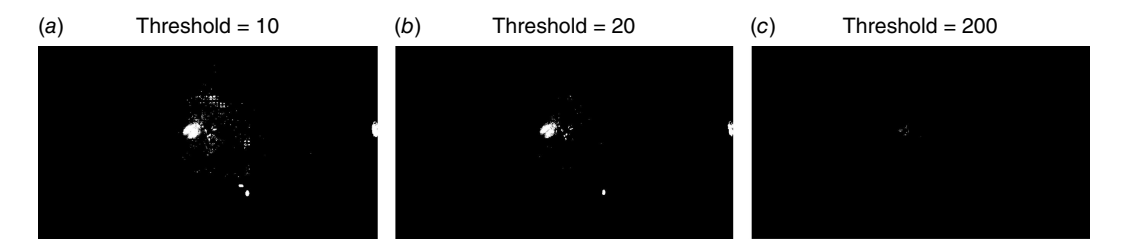


Fig. 4. Effect of different binary threshold values on the filtering process. Black (zero value) pixels represent the perceived background, while white (non-zero value) pixels represent pixels of interest that may contain the location of the firebrand. (a) Threshold value of 10, (b) threshold value of 20, and (c) threshold value of 200.

bark sample during combustion further complicate distinguishing between the object of interest and background artefacts. These smaller fragments exhibit unpredictable motion, often moving independently of the primary bark piece, creating additional noise points in the frame. Additionally, environmental elements unique to firebrands, like flickering flames or shifting smoke patterns, mimic movement and generate pixel changes in frame-difference calculations that are unrelated to the bark's trajectory. The irregular and chaotic movement of the main sample can further exacerbate the issue, as overlapping or merging regions of detected change complicate the isolation of the primary firebrand. Without effective filtering, the presence of these noise points can lead to false detections, inconsistent trajectories and inaccurate analyses of the bark's motion and combustion behaviour. Effective noise filtering techniques are thus essential to mitigate these challenges and ensure that only relevant points are retained for accurate trajectory tracking.

In the method applied here, the binary frame generated by applying a threshold to the difference frame isolates regions with significant pixel changes, known as pixels of interest. A binary threshold is applied to 8-bit greyscale frames (intensity range 0–255) to include or exclude pixels of interest, which is optimised based on the known size of the bark to minimise the number of noise points, including smaller released fragments,

while preserving the primary firebrand's features. Fig. 4 shows the effect of varying binary threshold values on the filtering process, where black has been identified as background (zero value pixels) and white is pixels of interest (non-zero pixel values) containing the firebrand, for thresholds of 10, 20 and 200 (arbitrary units). At a threshold of 10, the binary frame contains significant white pixels distributed throughout the image, representing excessive inclusion of irrelevant points. This level of noise makes identifying the firebrand highly inaccurate. Conversely, at a threshold of 200, the binary frame is over-filtered, with almost the entire image appearing black except for a few white pixels. This excessive filtering excludes critical information, making it unsuitable for effective tracking.

A threshold value of 20 was found through trial and error to strike the optimal balance, accurately highlighting the pixels of interest, including the bark, while minimising extraneous noise such as detached embers and reflections. This threshold serves as the foundation for the filtering process, providing a clean, repeatable and reliable input for subsequent tracking steps, where further refinement and noise reduction techniques are applied to ensure robust performance.

Non-zero pixels in the binary frame, representing potential firebrand locations, are stored in a cell array. To further reduce noise, candidate points are filtered based on their

proximity to the previously tracked bark sample centroid location, with only those within a specified distance – typically double the bark size – being retained. Outlier points are subsequently removed using a custom filtering function with predefined bounds, ensuring that noise is minimised and the tracking remains robust even in visually complex environments. This approach effectively isolates the main bark while addressing the challenges of smaller embers and environmental visual noise.

Reflections from acrylic windows

The reflective nature of the acrylic observation window surfaces in the working section, particularly from the topview camera, introduces a significant challenge. Reflections from these side windows can cause multiple appearances of the bark within the same frame, leading to false detections and complicating the tracking process. To address this issue, additional care is required during image analysis of the topview camera. An extra filtering step is introduced for this camera to distinguish actual bark positions from reflected counterparts. This step leverages geometric constraints and proximity-based filtering, ensuring that only points corresponding to the real firebrand location inside the working section are retained. This approach minimises the impact of reflections on tracking accuracy by identifying and removing reflections based on their inconsistent movement patterns or unlikely spatial positions relative to the known working section boundaries. Implementing such targeted filtering ensures robust and reliable tracking from the top view, even in the presence of reflective surfaces.

Conversion from pixel coordinates to Cartesian space

Owing to the 1.55° divergence angle in the shape of the working section, the optimal location for the origin reference point (i.e. zero reference) was set at the centre of the screen at the base of the working section. This ensured a consistent reference point for spatial measurements and minimised error during coordinate transformations. Although using data from two orthogonal camera views is sufficient to determine the x, y and z coordinates of the location of the centre of the firebrand sample, incorporating the average from all three orthogonal cameras reduces errors and enhances accuracy. In frames where the bark is occluded from either the front or left cameras owing to obstructions, such as the corners of the working section, data from the top camera and the other side camera, in which the bark sample is visible, can be used, albeit with lower accuracy. Coordinates common to both views are averaged, while the remaining coordinate is obtained from a single camera. Frames where the bark is visible only in the top view are excluded from analysis, as they do not provide sufficient information for 3D coordinate reconstruction.

By calibrating all cameras across different depths within the working section, pixel data from each view are converted into Cartesian coordinates relative to the origin. This calibration ensures accurate alignment of the coordinate systems and compensates for any distortion or misalignment, enabling precise tracking of the bark's position in 3D space.

Results and discussion

Understanding the trajectory of burning bark is crucial for predicting firebrand transport and potential spotting distances in bushfires. Tracking the trajectory of burning bark in a vertical wind tunnel provides valuable insights into its motion and behaviour under controlled airflow conditions. By capturing images from multiple orthogonal camera angles, the bark's position can be reconstructed in three dimensions for each frame and its trajectory analysed over sequential frames. This process enables researchers to study key parameters such as displacement, velocity and acceleration, which are essential for understanding how firebrands travel through the air. By analysing the movement of the bark while burning, researchers can also evaluate the effects of variables such as wind speed, bark size and combustion dynamics, contributing to a better understanding of spotting and secondary fire ignition mechanisms.

2D and 3D trajectory analysis

The bark samples listed in Table 1 were burned untethered in the vertical wind tunnel, allowing them to move freely within the controlled airflow until complete burnout. This setup enabled the observation of natural firebrand behaviour, including displacement, rotation and changes in shape due to combustion, and the results were used to evaluate the developed tracking methodology.

Fig. 5 illustrates an example of the output of the particle tracking process for sample No. 6 from the left- and front-view cameras. This figure shows the location of the burning bark sample within the working section (relative to the origin at the base of the working section) during the flight of the sample. The trajectory is coloured by the time of flight of the sample, from red when it was inserted into the airflow (at a speed close to the sample's terminal velocity), to blue at the end of the flight. As the bark burns, its shape and mass change, affecting its aerodynamic properties and ultimately influencing how far and fast it travels.

As identified previously, one limitation of using the frontand left-view cameras through the acrylic windows is that the bark can sometimes become obscured in the corners behind the edges of the window mounts, making it undetectable for several frames in one or both side cameras. The segmented trajectories, each defined by the first and last frames where the bark was visible in both camera views,

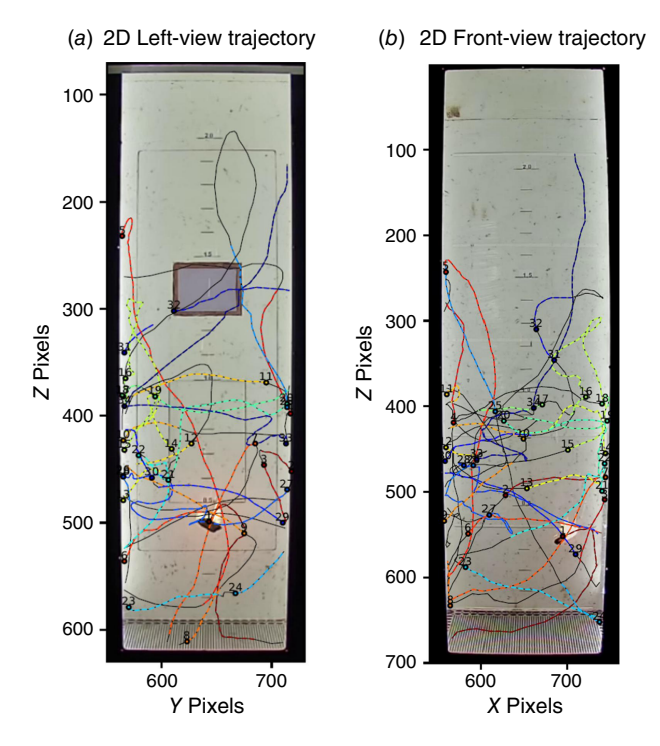


Fig. 5. Observed trajectory of bark sample No. 6. (a) Left view and (b) front view. Trajectories generated by both the left- and front-view cameras are shown as dashed lines, coloured by time of flight, red being at the start of the flight and blue being at the end of the flight with a gradient between. Solid black trajectories indicate where only one camera had a view of the sample. Numbers are the start of each segmented trajectory where the bark was visible in both camera views.

were plotted using a dashed line with a colour gradient where the first flight segment is dark red, representing the burning phase, and the final flight segment is blue, indicating burned out. If the bark was visible in one view but not the other, it was plotted as a solid black line.

Another limitation arises from the slight difference in camera positioning, as one camera is positioned slightly closer to the working section than the other. Additionally, a steel beam partially obstructs the view above the 2-m mark. This results in a minor difference in pixel scaling between the two views, making it difficult to align the images precisely when placed side by side, as shown in the figure. However, this discrepancy does not affect the accuracy of trajectory measurements or the determination of movement dynamics. It only influences visualisation, causing a slight height offset between the front and left views.

Fig. 6 presents the reconstructed 3D trajectory of bark sample No. 6 relative to the reference origin derived from the positional data in Fig. 5. This trajectory is divided into segments where each segment represents 1 s of movement and is plotted using the same colouring scheme as Fig. 5. The figure shows that the sample burned for a total of 40 s. This visualisation allows a clear understanding of how the bark moved and changed during its flight. The colour-coded segments also help to distinguish between the early burning phase and the

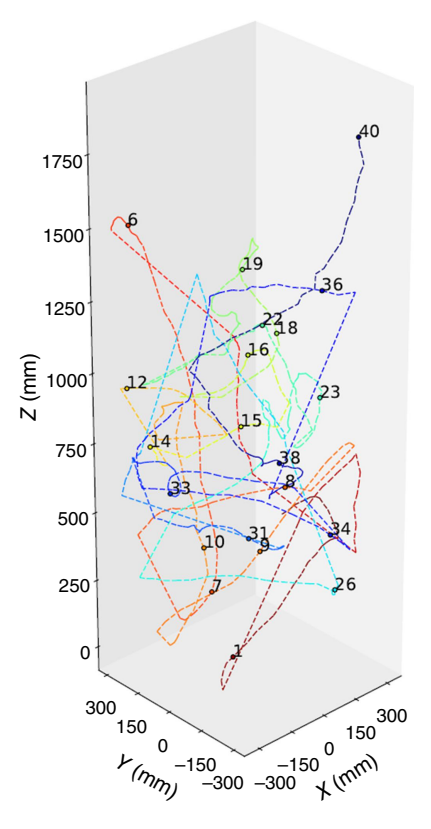


Fig. 6. Compiled 3D trajectory of the sample bark No. 6 derived from positional data given in Fig. 5. Each second of sample flight defines a numbered segment drawn as a dashed line that is coloured by time since commencement from red at the start (t = 0 s) to blue at the end (t = 40 s).

final stages approaching burnout, offering a more detailed and insightful analysis of firebrand dynamics. This method of segmentation and visualisation is crucial for improving our understanding of firebrand behaviour in wildfire scenarios, and can easily be applied to future experiments involving different fuel types or varying environmental conditions.

A quantitative comparison of the 3D point cloud generated by the tracking algorithm and that derived from the accurate, manually-annotated 2D coordinates from synchronised frames was carried out to validate and assess the results of the tracking algorithm. The average positional error was found to be approximately \pm 23 mm in the x-axis, \pm 12 mm in the y-axis and \pm 36 mm in the z-axis. These correspond to relative errors of approximately 4, 2 and 2% along the x, y and z axes, respectively, indicating a high level of accuracy in the automated tracking algorithm for identifying the position of the firebrand sample in each frame and thus giving high confidence in the reconstruction of the sample's 3D trajectory and subsequent analysis of firebrand velocity components.

Velocity estimation

The calculated velocities of sample No. 6, v_x , v_y , v_z and the total velocity v_t relative to the origin reference and derived

from the data in Fig. 6, are plotted as a time series for its flight in Fig. 7, showing how the particle's motion evolved during the experiment while it burned. These velocity components represent the bark's movement in the x (blue), y (green) and z directions (red), while v_t (black) represents the magnitude of the total velocity vector (i.e. the vector sum of v_x , v_y , v_z). By examining these plots, we can observe how airflow, combustion and any changes in shape or mass influenced the bark's dynamics during its flight.

The velocity profiles reveal valuable insights into the forces acting on the bark as it burns. Fluctuations in the individual components may indicate oscillatory motion, tumbling, or aerodynamic instabilities, while the trend of ν_t helps identify phases of rapid acceleration or deceleration relative to the overall air flow. For instance, a gradual decrease in ν_t might correspond to mass loss or reduced lift as the bark burns out.

The v_x and v_y components lie in the horizontal plane perpendicular to the airflow and capture the sideways motion of the bark during flight. When v_z is zero, it indicates that the

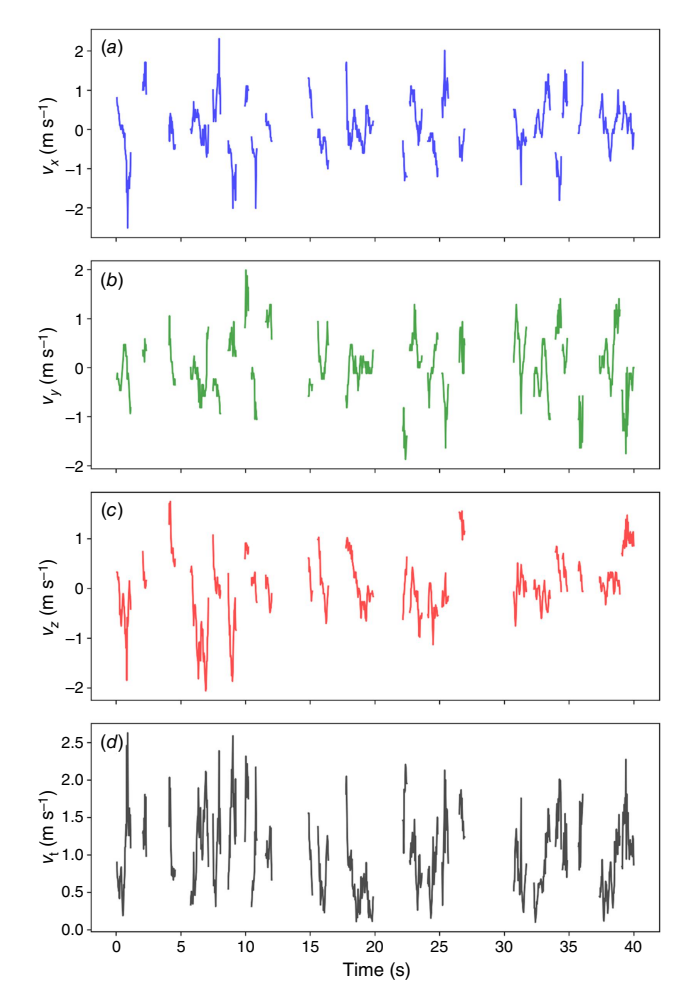


Fig. 7. Time series of relative velocity components of the burning bark sample: (a) v_x (blue), (b) v_y (green), (c) v_z (red), and (d) the total velocity v_t (black) for flight of sample No. 6 while burning.

bark has reached a vertical position in the wind tunnel where the local air speed matches its terminal velocity.

By identifying these frames and correlating them with the corresponding bark sample positions and fan speeds, we can gain deeper insight into the conditions under which the bark achieves terminal velocity while burning. Additionally, $\nu_{\rm t}$ provides a complete view of the sample's overall motion in the airflow.

A box plot (Fig. 8) is used to visualise the velocity distribution of the velocity components given in Fig. 7 over the entire burning period of the sample. This alternative representation offers a statistical summary of the data, highlighting the central tendency, variability and presence of any outliers. The horizontal velocity components (v_x and v_y) show wider interquartile (IOR) ranges, indicating relatively unstable lateral motion of the sample, possibly due to the influence of turbulence, asymmetries in the bark shape, or slight variations in how the sample was introduced into the airflow. In contrast, the vertical velocity component (v_z) displays a narrower spread, reflecting more stability in the upward or downward motion. This behaviour arises because a bark sample tends to oscillate around the height where the tunnel air speed is close to its terminal velocity. Consequently, while the fluctuations in v_z in this example are limited, a bark sample can still undergo substantial vertical displacement over time, often larger than the transverse displacement. This highlights the fact that a narrower vertical velocity spread does not imply restricted vertical movement but rather reflects the balance between air forcing and particle terminal velocity. The airflow in the wind tunnel likely plays a key role in stabilising the vertical motion, especially after the initial ignition and insertion into the flow and as the bark settles into a balanced state of lift and drag while burning.

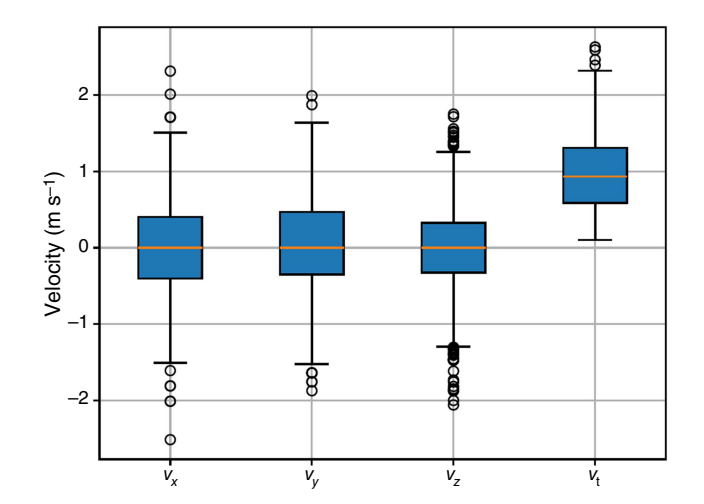


Fig. 8. Box plot showing the distribution of the relative velocity components v_x , v_y , v_z and the total velocity v_t for bark sample No. 6 while burning. Each box represents the interquartile (IQR) range (25th to 75th percentile), with the orange line indicating the median velocity. Whiskers extend to the minimum and maximum values within 1.5 times the IQR range, while points outside this range are outliers.

The total relative velocity (v_t) box plot provides an overall sense of how the bark behaved aerodynamically throughout its combustion. A higher median value or wide range in v_t may suggest periods of rapid movement, such as during the initial insertion or when turbulent airflow interacts with the irregular shape of the bark. Outliers in any of the velocity components may correspond to abrupt changes in motion – possibly due to combustion-driven deformation, tumbling, or sudden lift fluctuations. Compared with the time-series plots, the box plot offers a compact, at-a-glance view of velocity behaviour and variability, which is particularly useful when comparing multiple samples or testing the effects of different airflow conditions or ignition methods.

Fig. 9 presents smoothed velocity–time distributions for each of the 10 individual bark samples listed in Table 1. Each line represents the time each sample spent in specific velocity categories or bins while visible in both the left- and front-view cameras – *not* the total flight time. The legend includes the total flight time for each sample, demonstrating substantial variation between them, from as little as 17 to over 100 s. The thick black line represents the average distribution of velocities of all samples, providing a useful comparative baseline.

The individual velocity distributions exhibit peaks typically less than $1.0~{\rm m~s}^{-1}$, indicating most are reaching a stable behaviour at or near the sample's terminal velocity, with long tails extending toward higher velocities. This trend reflects the range of aerodynamic behaviours during free fall. The plot offers a clear yet nuanced view of firebrand dynamics, highlighting both common behaviours and individual variability in the burning and motion behaviour of the bark samples.

Combustion phase classification

The top-view camera is used to monitor and define the different phases of combustion by capturing changes in the appearance

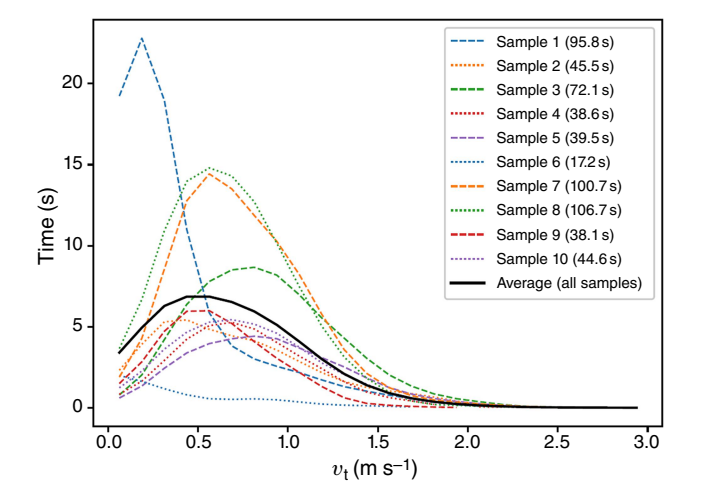


Fig. 9. The smoothed velocity–time distributions for 10 burning samples. The visible time is \sim 25–60% of the total burning time given in the legend.

of the burning bark from above. The burning process is classified into three combustion phases: flaming, glowing or smouldering and burnout. Flaming combustion involves gas-phase oxidation of volatiles released in the thermal degradation of the sample, evident as flame (Sullivan and Ball 2012). Glowing combustion involves solid-phase oxidation of the char formed during the thermal degradation of the sample, evident either as faint red radiance or the release of particulate-laden smoke (Sullivan and Ball 2012). Burnout is not a combustion phase as such, but provides a brief period during the experiment to provide confidence that combustion has indeed ceased and the sample will not recommence burning.

The information generated from the combustion phase classification provides valuable insights into the progression of combustion, particularly in distinguishing between the phases. However, this approach has certain limitations. One significant issue is the temporal overlap of the flaming and glowing phases, where the transition between the two can be gradual or occur at different locations on the bark sample, making it difficult to clearly define their boundaries during flight. Additionally, the natural rotation of the bark during combustion introduces further challenges. When the flaming part of the bark moves to the bottom owing to rotation, it becomes obscured from the top camera's view, potentially leading to missed detections of active flaming and misclassification of combustion phase. These limitations highlight the need for supplementary methods to improve the accuracy of phase identification, especially in dynamic burning scenarios. The statistical analysis of the duration of each phase provides insight into the temporal dynamics of the progression of the sample's combustion, as shown for the complete set of 10 firebrand samples in Fig. 10.

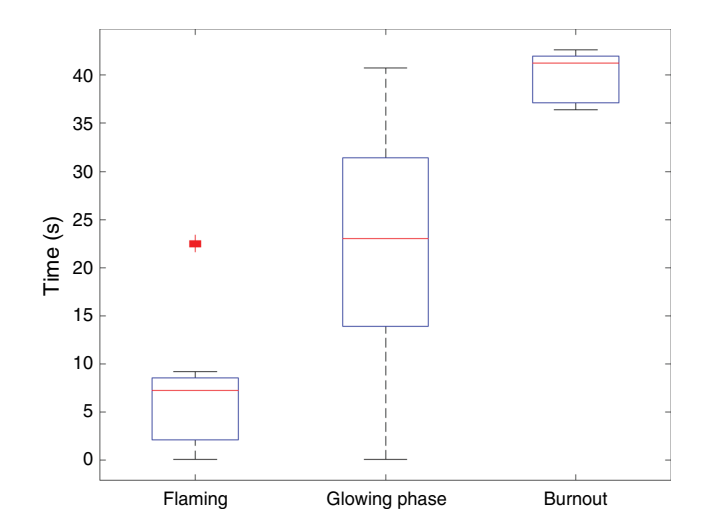


Fig. 10. Box plot showing variations in duration of the different combustion phases observed in the set of 10 bark samples. Each box represents the IQR range (25–75th percentile), with the orange line indicating the median velocity. Whiskers extend to the minimum and maximum values within 1.5 times the IQR range, while points outside this range are outliers.

As it is ignited using flame, the flaming phase always occurs early in the process, with a median duration of ~ 7 s. The range of the flaming phase duration spans from insertion to a maximum of ~ 12 s after insertion. The IQR range, which lies between the 25th percentile and the 75th percentile, for the flaming phase of the set of samples shows that most of the flaming events occur within this time range. The phase duration is relatively short, as evidenced by the narrow spread between the minimum and maximum values. However, the phase exhibits significant variability, as shown by the relatively wide range of durations. A total of 21 outliers were identified in this phase, suggesting some instances of reflaming and inconsistency in the manner of flaming combustion.

The glowing phase typically immediately follows the flaming phase and represents a longer, less intense part of the combustion process. The median duration of the glowing phase is ~21 s, with a range from insertion to the end. The IQR for this phase extends from 12 s (25th percentile) to 30 s (75th percentile) after insertion, indicating that most glowing occurs within this time window. Notably, there were no outliers in the glowing phase, suggesting a more consistent duration compared with the other phases. The glowing phase had the largest number of data points, indicating that it is the predominant phase observed during the burning process.

Finally, the burnout phase occurs at the end of the burning sequence and is marked by the extinction of visible combustion. This phase has a median duration of 5 s, with a range extending from a minimum of $12 \, s$ to the end of the experiment. The IQR for the burnout phase ranges from approximately $35 \, s$ ($25 \, th$ percentile) to $40 \, s$ ($75 \, th$ percentile) after insertion, indicating that most burnout durations are concentrated toward the end of the process.

Conclusion

This study developed and evaluated a valuable method for capturing high spatial and temporal resolution data on the combustion and flight dynamics of burning, untethered firebrand samples while in free fall in an airstream within a vertical wind tunnel. The firebrand tracking methodology employs multiple orthogonal and synchronised cameras to capture firebrand position and combustion phase over time, which it uses to reconstruct the 3D trajectory and combustion progression of firebrand samples. The method enables detailed analysis of a firebrand's displacement, component and total velocities, and acceleration over time. Despite some challenges, including partial occlusions caused by the experimental setup and minor misalignments between the camera views resulting in pixel scaling differences between the camera views, the results were shown to be highly accurate, with a mean error in position of 4% or less.

The study's key contribution lies in the segmentation and visualisation of the 2D and 3D trajectories, which provided a clear representation of the flight characteristics as well as the combustion behaviours. These visualisations allow a detailed understanding of the firebrand's behaviour during its transport, including how the combustion process and aerodynamic forces affect its motion.

The velocity data, including both time-series and frequency distribution representations, further enhanced this analysis, revealing fluctuations in lateral and vertical motion that may be indicative of the firebrand's interaction with the airflow and changes in its shape and mass during combustion. Such analysis provides potential for a comprehensive understanding of a firebrand's aerodynamic behaviour. Visualising the variability and stability of these movements across multiple samples under different conditions is crucial for improving predictive models of firebrand transport and spotting behaviour in wildland fires.

Although this study focused on the kinematics of individual firebrands, the outputs – including 3D trajectories, terminal velocity and velocity components, flaming durations and burnout times – can be used to advance both wildland fire spread and wildland–urban interface (WUI) fire modelling. These data enable the improved parameterisation of existing firebrand transport models and open the possibility for the development of improved, bespoke firebrand transport models. Such improved models will create more accurate predictions of spotting distances, particularly important when wildland fires transition into urban areas, and better estimation of the spotting potential of firebrands in general wildfire spread simulations.

Although a deep analysis of these behaviours is beyond the scope of this paper, the results presented here illustrate the robustness of the automated tracking methodology, including validation of the consistency of velocity extraction across multiple samples and assessment of the algorithm's ability to handle partial occlusions and visibility loss. Detailed interpretation of the aerodynamic or combustion dynamics will be addressed in future studies, particularly through the incorporation of additional environmental variables, refining tracking techniques and exploration of different firebrand types, morphologies and combustion behaviours. Ultimately, the objective of this research is to advance our understanding of firebrand dynamics, providing data that can inform strategies to mitigate the spread of bushfires in both urban and rural areas.

References

Abdelaziz M, Sullivan A (2024) The modification and characterisation of the CSIRO vertical wind tunnel for the study of untethered free-falling firebrands. In 'Proceedings of the 24th Australasian Fluid Mechanics Conference (AFMC)'. Canberra, Australia. Paper No. AFMC2024-299. doi:10.5281/zenodo.14213598

Almeida M, Porto L, Viegas D (2021) Characterization of firebrands released from different burning tree species. *Frontiers in Mechanical Engineering* **7**, 651135. doi:10.3389/fmech.2021.651135

- Bathija A, Sharma G (2019) Visual object detection and tracking using YOLO and SORT. *International Journal of Engineering Research Technology* **8**(11), 345–355.
- Bouvet N, Link ED, Fink SA (2021) A new approach to characterize firebrand showers using advanced 3D imaging techniques. *Experiments in Fluids* **62**(9), 181. doi:10.1007/s00348-021-03277-6
- Carranza F, Zhang Y (2017) Study of drag and orientation of regular particles using stereo vision, Schlieren photography and digital image processing. *Powder Technology* **311**, 185–199. doi:10.1016/j.powtec. 2017.01.010
- Cruz M, Sullivan A, Gould J, Sims N, Bannister A, Hollis J, Hurley R (2012) Anatomy of a catastrophic wildfire: the Black Saturday Kilmore East fire in Victoria, Australia. Forest Ecology and Management 284, 269–285. doi:10.1016/j.foreco.2012.02.035
- Cruz MG, Gould JS, Alexander ME, Sullivan AL, McCaw WL, Matthews S (2015) Empirical-based models for predicting head-fire rate of spread in Australian fuel types. *Australian Forestry* **78**(3), 118–158. doi:10.1080/00049158.2015.1055063
- Diwan T, Anirudh G, Tembhurne JV (2023) Object detection using YOLO: challenges, architectural successors, datasets and applications. *Multimedia Tools and Applications* **82**(6), 9243–9275. doi:10.1007/s11042-022-13644-y
- Ellis P (2010) The effect of the aerodynamic behaviour of flakes of jarrah and karri bark on their potential as firebrands,. *Journal of the Royal Society of Western Australia* **93**, 21–27.
- Ellis P (2011) Fuelbed ignition potential and bark morphology explain the notoriety of the eucalypt messmate 'stringybark' for intense spotting. *International Journal of Wildland Fire* **20**(7), 897–907. doi:10.1071/WF10052
- Ellis P (2013) Firebrand characteristics of the stringy bark of messmate (*Eucalyptus obliqua*) investigated using non-tethered samples. *International Journal of Wildland Fire* **22**(5), 642–651. doi:10.1071/WF12141
- Ellis P (2015) The likelihood of ignition of dry-eucalypt forest litter by firebrands. *International Journal of Wildland Fire* **24**(2), 225–235. doi:10.1071/WF14048
- Ellis PF (2000) The aerodynamic and combustion characteristics of eucalypt bark: a firebrand study. PhD Thesis, Department of Forestry, The Australian National University, Canberra, ACT, Australia. doi:10.25911/5D7A2814C478D
- Filkov A, Prohanov S (2019) Particle tracking and detection software for firebrands characterization in wildland fires. *Fire Technology* **55**, 817–836. doi:10.1007/s10694-018-0805-0
- Filkov AI, Tihay-Felicelli V, Masoudvaziri N, Rush D, Valencia A, Wang Y, Blunck DL, Valero MM, Kempna K, Smolka J, et al. (2023) A review of thermal exposure and fire spread mechanisms in large outdoor fires and the built environment. Fire Safety Journal 140, 103871. doi:10.1016/j. firesaf.2023.103871
- Hall J, Ellis PF, Cary GJ, Bishop G, Sullivan AL (2015) Long-distance spotting potential of bark strips of a ribbon gum (*Eucalyptus viminalis*). *International Journal of Wildland Fire* **24**(8), 1109–1117. doi:10.1071/WF15031

- Hines F, Hines F, Tolhurst KG, Wilson AA, McCarthy GJ (2010) Overall Fuel Hazard Assessment Guide. Fire and Adaptive Management Report No. 82. (Victorian Government Department of Sustainability: Melbourne, Vic, Australia)
- Knight I (2001) The design and construction of a vertical wind tunnel for the study of untethered firebrands in flight. *Fire Technology* **37**(1), 87–100. doi:10.1023/A:1011605719943
- Knight I, Ellis P, Sullivan A (2001) The CSIRO Vertical Wind Tunnel. (CSIRO Forestry and Forest Products: Canberra, ACT, Australia)
- Koo E, Pagni PJ, Weise DR, Woycheese JP (2010) Firebrands and spotting ignition in large-scale fires. *International Journal of Wildland Fire* 19(7), 818–843. doi:10.1071/WF07119
- MATLAB (2023) Version 23.2.0 (R2023b). (The MathWorks Inc.: Natick, MA, USA)
- McArthur AG (1967) 'Fire behaviour in eucalypt forests.' Forestry and Timber Bureau Leafet 107. (Commonwealth Department of National Development: Canberra, ACT, Australia)
- McArthur AG (1969) The Tasmanian bushfires of 7th February, 1967, and associated fire behaviour characteristics. In 'Mass Fire Symposium', 10–12 February 1969, Collected Papers. 24 p. (Defence Standards Laboratory: Maribyrnong, Vic, Australia)
- Petersen AJ, Banerjee T (2024) Characterizing firebrands and their kinematics during lofting. *Physics of Fluids* **36**(10), 106611. doi:10.1063/5.0227024
- Prevost CG, Desbiens A, Gagnon E (2007) Extended Kalman filter for state estimation and trajectory prediction of a moving object detected by an unmanned aerial vehicle. In '2007 American Control Conference'. pp. 1805–1810. (IEEE: New York, NY, USA)
- Sullivan A, Ball R (2012) Thermal decomposition and cobustion chemistry of cellulosic biomass. *Atmospheric Environment* **47**, 133–141. doi:10.1016/j.atmosenv.2011.11.022
- Sullivan AL (2017) Inside the inferno: fundamental processes of wildland fire behaviour. Part 2: Heat transfer and interactions. *Current Forestry Reports* 3, 150–171. doi:10.1007/s40725-017-0058-z
- Sullivan AL, McCaw WL, Cruz MG, Matthews S, Ellis PF (2012) Fuel, fire weather and fire behaviour in Australian ecosystems. In 'Flammable Australia: Fire Regimes, Biodiversity and Ecosystems in a Changing World'. (Eds RA Bradstock, AM Gill, RD Williams) pp. 51–77. (CSIRO Publishing: Melbourne, Vic, Australia)
- Tohidi A, Kaye NB (2017) Aerodynamic characterization of rod-like debris with application to firebrand transport. *Journal of Wind Engineering and Industrial Aerodynamics* **168**, 297–311. doi:10.1016/j.jweia.2017. 06.019
- Tolhurst KG, Cheney NP (1999) Synopsis of the knowledge used in prescribed burning in Victoria. (Department of Natural Resources, Environment)
- Wadhwani R, Sullivan C, Wickramasinghe A, Kyng M, Khan N, Moinuddin K (2022) A review of firebrand studies on generation and transport. *Fire Safety Journal* **134**, 103674. doi:10.1016/j. firesaf.2022.103674
- Zhejiang Uniview Technologies Co., Ltd. (2021) EZStation [computer software]. Available at https://www.uniview.com.

Data availability. The data used in this study will be made available on reasonable request to the corresponding author.

Conflicts of interest. Andrew Sullivan is an Associate Editor for the *International Journal of Wildland Fire* but was not involved in the peer review or decision-making process for this paper. The authors have no further conflicts of interest to declare.

Declaration of funding. This research did not receive any specific funding.

Acknowledgements. The authors would like to thank Alberto Alonso Pinar for his assistance with bark collection and help during the experimental setup, as well as Matt Plucinski, Mark Kitchen and Marek Tuhy. We acknowledge the Ngunnawal and Ngambri peoples, who are the Traditional Custodians and knowledge holders of the Country on which we conducted this research.

Author affiliation

^ACSIRO, GPO Box 1700, Acton, Canberra, ACT 2601, Australia.

Appendix 1. Tracking algorithm

Syncing the videos

Figs A1–A3 show the process of verifying the consistency of the synchronisation; we check the frame alignment when the lights are turned on and off. After this, the videos are trimmed to start just after the hatch is closed – following the placement of the burning bark into the wind tunnel's test section using tongs – ensuring that the bark appears at the same moment across all three camera views.

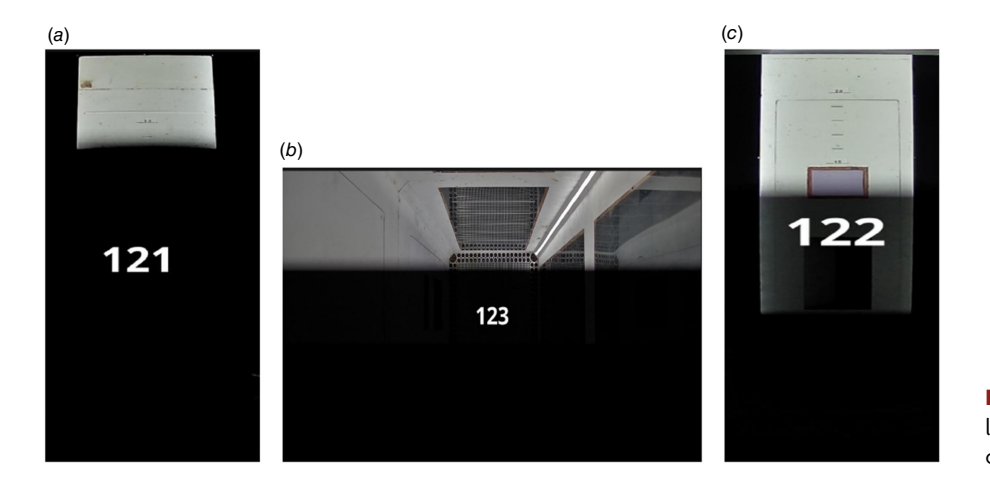


Fig. A1. The first frame of turning the LED lights off: (a) is the front camera, (b) is the top camera, and (c) is the left camera.

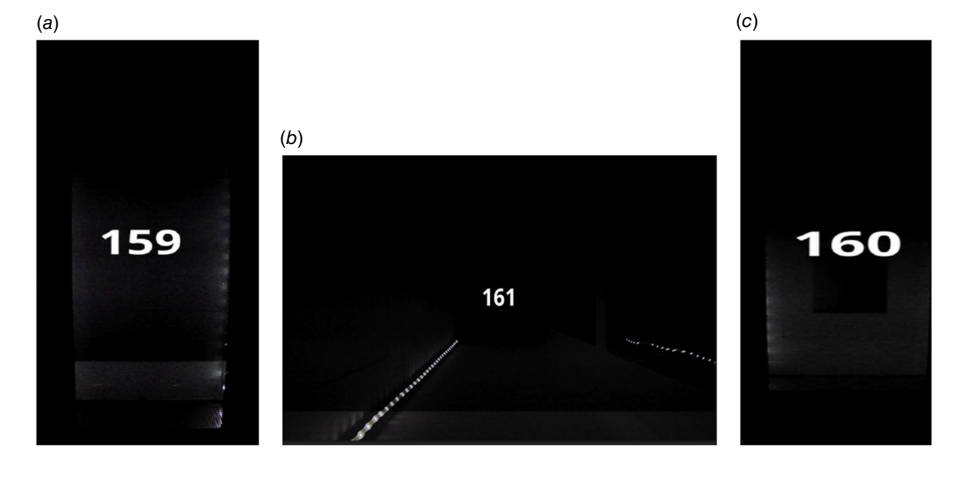


Fig. A2. The first frame of turning the LED lights on again: (a) is the front camera, (b) is the top camera, and (c) is the left camera.

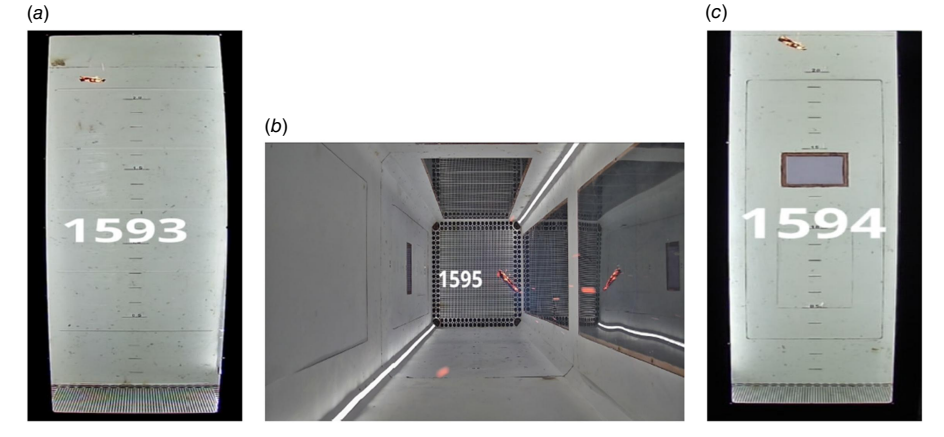


Fig. A3. Random frame after syncing the videos while burning the bark: (a) is the front camera, (b) is the top camera, and (c) is the left camera.

Final result

Fig. A4 shows the final points array after filtering all the noise and inaccurate points with blue dots and the centre point with green stars.



Fig. A4. The final points array after filtering all the noise and inaccurate points with blue dots and the centre point with green star.

Fig. A5 shows a random frame with different cameras simultaneously of an untethered, burning, free-falling firebrand. The origin point and the coordinate directions are shown in each camera view.

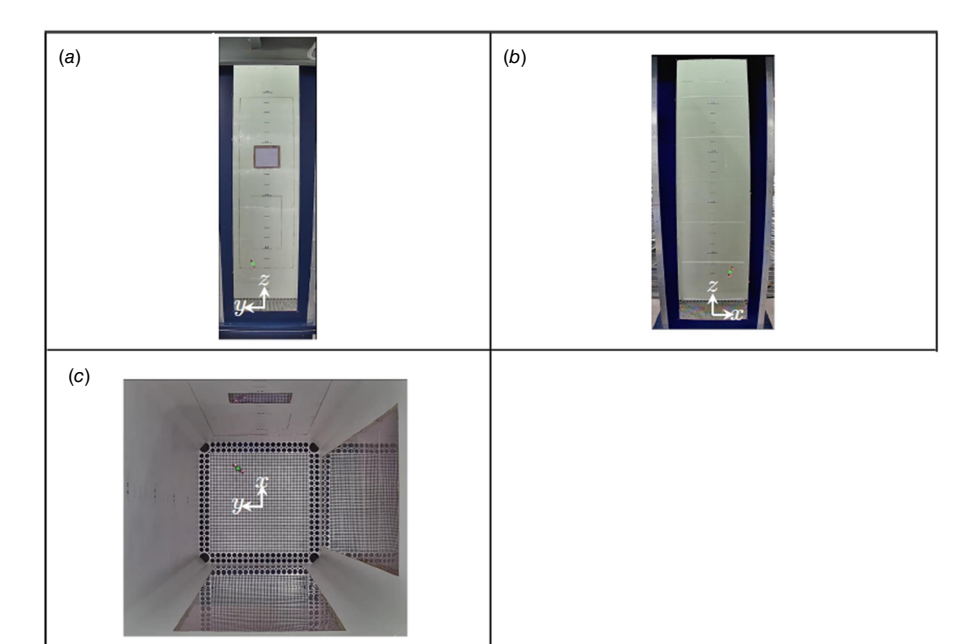


Fig. A5. A random frame from the multiple-camera system of an untethered, burning, free-falling firebrand: (a) left side view, (b) front view, and (c) top view.